The effect of intermediate frequency on sheath dynamics in collisionless current driven triple frequency capacitive plasmas

S. Sharma[*1]**, S. K. Mishra**[1, 2]**, P. K. Kaw**[1] **and M. M. Turner**[3]

[1] *Institute for Plasma Research* (IPR)*, Gandhinagar, India*

[2] *ELI-ALPS, Szeged, Hungary*

[3] *National Centre for Plasma Science & Technology, Dublin City University, Ireland*

Abstract

The CCP (*Capacitively Coupled Plasma*) discharge featuring operation in current driven triple frequency configuration has analytically been investigated and the outcome is verified by utilising 1D3V *particle-in-cell* (*PIC*) simulation code. In this analysis the role of middle frequency component of the applied signal has precisely been explored. The discharge parameters are seen to be sensitive to the ratio of the chosen middle frequency to lower and higher frequencies for fixed amplitudes of the three frequency components. On the basis of analysis and PIC simulation results, the middle frequency component is demonstrated to act as additional control over sheath potential, electron sheath heating and *ion energy distribution function* (*iedf*) of the plasma discharge. For the electron sheath heating, effect of the middle frequency is seen to be pronounced as it approaches to the lower frequency component. On the other hand for the *iedf*, the control is more sensitive as the middle frequency approaches towards higher frequency. The PIC estimate for the electron sheath heating is found to be in reasonably good agreement with the analytical prediction based on *Kaganovich* formulation.

* *Author's E-mail: sarvsarvesh@gmail.com*

The efficacy of operating capacitively coupled plasma (CCP) discharges at low pressure (~*mTorr*) configuration, makes it a promising tool (*e.g.* as a plasma source for etching and thin film deposition) for microelectronics industry in the fabrication of large scale integrated circuits[1-5]. In material processing, uniform etching/ deposition over the electrode, and control over sheath plasma parameters, ion flux and energy are essential[1]. In case of conventional CCP source the discharge is driven by a single frequency source and all these parameters are coupled to each other. Thus it is not possible to individually control the various plasma discharge features in conventional CCP discharges[3-5]. In contrast, the recent studies[5-9] elucidate that such discrete control over plasma discharge features can be obtained by using non-harmonic, tailored or multi frequency signals over discharge electrodes. This fact is further supported by numerous analytical works based on hydrodynamic modelling[10-13], simulation (fluid & PIC) studies[14-16] and experimental campaigns[17-19].

Dual frequency (*df*-) CCP discharge, proposed by *Goto et al.*[20-21] is an example of controlled discharge operation where simultaneously operative high and low frequency RF signals are used to separately control the plasma density (ionization) and ion energy (bias voltage). Using *PIC Monte Carlo collision* (*PIC-MCC*) simulation, *Georgieva et al.*[22] demonstrated that the ion energy distribution function (*iedf*) gets broadened when the fundamental frequency (27*MHz*) is used together with low frequency source (1-2*MHz*); the broadening is observed to be large in case of 1*MHz* than that of 2*MHz*. It is also noticed that the average ion energy is driven by time averaged voltage across the sheath which itself is sensitive to the applied signal voltage and frequency ratios. From the existing studies it is known that in the high frequency regime (*say*), the system length may exceed the excitation wavelength and may lead to a distorted *iedf*, resulting in the non-uniformity near electrodes. For example, an increase in high frequency signal voltage leads to the shift of *iedf* towards higher energy and may damage surface material. On the other hand, decrease in low frequency signal voltage results in shifting of *iedf* towards lower energy and weakens the plasma etching rate[22-28]. In recent studies[29] it is proposed that distortion in energy extremes which arises in *df-CCP* can be tackled (*i.e.* by controlling *iedf*) by introducing an intermediate frequency with *df*-CCP discharge configuration. Furthermore[23-26], non-sinusoidal signals (configured with multiple harmonics) and tailored waveforms have also been used for more efficient control of discharge operations (i.e. fine tuning of ion energy and ion flux and hence *iedf*). The applicability of such configurations is limited because of the coupling between applied multiple harmonics which might lead to an asymmetric plasma response. A detailed analysis of merits and limitations of the use of non-sinusoidal waveforms in CCP discharges may be found in the elegant review by *Lafluer*[27].

In this paper we would like to systematically discuss the stochastic heating and *iedf* control in the case of triple frequency CCP (*tf-CCP*). The effect of mid frequency insertion in *tf-CCP* has been illustrated by various numerical simulation techniques[29-32] but most of the analysis so far has been restricted to a homogeneous sheath modelling[33] and far from realistic sheath features. It is only recently that *Rehman & Dewan*[34] have taken account of sheath inhomogeneity following the *Lieberman's*[35] analysis. In particular, the sheath dynamics has been examined in terms of instantaneous sheath position and mean potential. In low pressure regime, collisionless heating of the electrons is the dominant mechanism of energy transport/ deposition in the vicinity of the sheath. This heating primarily ensues as a consequence of mutual interaction between expanding/ collapsing phase of the sheath in response to the applied oscillatory *RF* field[36]. This effect has been verified experimentally[37-38] and by simulation techniques[45-50]. In present analysis, we intend to investigate the characteristic features of CCP discharge operating with triple frequency source in current driven mode. The current driven mode is chosen here because in present analysis we use Lieberman[35] model as a standard approach and investigate how use of multiple frequency modifies these results. Current driven mode also simplifies the problem by artificially switching off the plasma series resonance effect which can contribute significantly to electron heating in CCP discharges[1,35,40]. We anticipate that in *tf-CCP* case scaling of average sheath potential and ion energy (etching rate), by adjusting the intermediate frequency should be possible. First this has been examined by an analytical formulation and after that it is further verified with a self-consistent 1*D-multiple port electrostatic particle in cell* (PIC) simulation code. The outcome may provide an insight for designing the laboratory experiments and may also be helpful for industrial applications.

To get a physical insight of the problem, we establish an analytical formulation for the *CCP* discharge operating in low pressure collisionless regime with a triple frequency current driven signal. The algebraic form of the transient profile associated with applied triple frequency current source can be written as

$$j(x) = \left[j_l sin\omega_l t + j_m sin(\omega_m t + \theta_m) + j_h sin(\omega_h t + \theta_h) \right], \qquad (1a)$$

$$\Rightarrow j(x) = j_l \left[sin(\omega_l t) + c_{ml} sin(\alpha\omega_l t + \theta_m) + c_{hl} sin(\beta\omega_l t + \theta_h) \right] = j_l f_o, \qquad (1b)$$

where j, $\omega(=2\pi f)$ and θ are the amplitude, frequency and phase of the applied current source, the subscripts *l, m and h* refer to lower, intermediate and highest frequency components of applied signal, $\alpha = \omega_m / \omega_l$, $\beta = \omega_h / \omega_l$, $c_{ml} = j_m / j_l$ & $c_{hl} = j_h / j_l$ with $j_l = 4A/m^2, j_m = 20A/m^2, j_h = 40A/m^2$ and $f_l = 2MHz, f_m = 16MHz, f_h = 80MHz$; other simulation parameters are described in subsequent sections. It should be noted here, that experimental reactors operating in low pressure regime are geometrically asymmetric[51-65] and thus the current form may significantly differ from the algebraic form stated in Eq.1. In fact, use of multiple harmonic signals over electrodes causes electrical asymmetry and sets a finite dc field between the electrodes[2-4]. Consequently, the sheath response modulates the *iedf* which effectively reflects the ion flux and energy available for deposition. This asymmetry can be regulated up to a desired extent by adjusting the frequency and phase between externally applied signals that gives additional control over discharge confinement and relevant plasma parameters. Nevertheless, concerning our prime emphasis in this paper on exploring the influence of the intermediate frequency in the CCP discharge and comparison with well known analytical models[31,36], we confine our analysis to symmetric electrode system only.

The temporal profile of the applied signal in *single frequency* (*sf*), *dual frequency* (*df*) and *triple frequency* (*tf*) mode are illustrated in figures (Fig.2a). In simulation, pulse train has been applied to the electrodes and system is left to evolve and attain steady state situation; the steady state features of the discharge parameters over a complete *RF* cycle has graphically been illustrated. The sheath dynamics in CCP discharge operating in *tf* configuration, eventually depends upon the cumulative current profile modulated due to frequency manifestation of all the three signals; we follow the analysis by *Lieberman*[35] and *Kaganovich et al.*[40] to establish the expressions for sheath parameters and heating of electrons in the next section (*i.e. Section*-2). The third section (*i.e. Section*-3) includes the description of 1*D-multiple port electrostatic particle-in-cell* (PIC) simulation code and parameters used for the computations. The physical interpretation and discussion of the numerical results based on analysis has been given in *Section*-4. Finally, a summary of the outcome in section-5 concludes the paper.

2. *Analytical modelling: Sheath structure and collisionless sheath heating of electrons*

In this section utilizing the formalism adopted by *Lieberman*[35] and *Kaganovich et al.*[40], we derive the expressions for sheath structure and consequent collisionless heating of the electrons in the proximity of the sheath region in a *CCP* discharge, driven by triple frequency setup. To get a clear idea about the conceptual features of the discharge, a schematic of *tf* configuration of CCP discharge in current driven mode (*similar to reference* 33) has been displayed in Fig.1a. Following *Lieberman*[35], the *Poisson* equation for the instantaneous electric field (E) in the sheath region can be expressed as

$$\begin{aligned} (\partial E/\partial x) &= (e/\varepsilon_0)n_i(x)\,, && s(t) < x \\ &= 0 && s(t) > x \end{aligned} \qquad (2)$$

Here $s(t)$ refers the distance from ion sheath edge (at $x = 0$) to electron sheath edge, x is an arbitrary position in the sheath region, $n_i(x)$ is the axial ion density, ε_0 is permittivity of free space and e refers the electronic charge (*see* Fig.1b, *Ref.*17). Here, we have taken simplified RF electron sheath model (step function) given by *Lieberman*[35] for analysis. In recent works (*e.g. Brinkmann*[65]) by using a more sophisticated electron sheath model, the presence of significant electric field in the bulk-sheath transition region is visualized which in turn also perceived to contribute in electron sheath heating[66-67]. However, concerning our motivation to explore the influence of intermediate frequency on discharge features, as the first step we keep our case simple and use *Lieberman*[35] and *Kaganovich et al.*[40] approach for the analysis. Manifesting the Poisson equation with number and energy conservation of ions in the sheath region, the equations for the parameters governing sheath structure *viz.* for the mean electric field, electric potential, and electron/ ion density can be expressed as[35]

$$(d\overline{E}/dx) = (e/\varepsilon_0)\left[n_i(x) - \overline{n}_e(x)\right], \tag{3}$$

$$(d\overline{\varphi}/dx) = -\overline{E}, \tag{4}$$

$$\overline{n}_e(x) = [1-(\gamma/\pi)]n_i(x), \tag{5}$$

and

$$n_i(x) = n_0(1-2\overline{\varphi}/T_e)^{-1/2}, \tag{6}$$

where E, φ and n_e / n_i are the electric field, potential and electron/ ion density respectively, n_0 is the mean density of electrons/ions in bulk (ion sheath edge) and γ refers to arbitrary phase associated with position x in the sheath region; the bar on these quantities correspond to the time average values over one *RF* cycle. The motion of the instantaneous electron sheath which is driven by applied current signal, can be written as

$$n_i(x)u_s = n_i(x)(ds/dt) = j(x) = \left[j_l sin\omega_l t + j_m sin(\omega_m t+\theta_m) + j_h sin(\omega_h t+\theta_h)\right], \tag{7}$$

where u_s is the velocity of the electron sheath edge.

Following the algebraic steps given in *Ref.*35, one can combine the space and time integrations of *Eq.*(2) and *Eq.*(7) respectively to obtain the instantaneous electric field as

$$\begin{aligned} E(x,\omega t) &= \frac{e}{\varepsilon_0}\int_0^x n_i(\varsigma)d\varsigma \\ &\quad -\frac{1}{\varepsilon_0}\left[\frac{j_l}{\omega_l}(1-Cos\omega_l t) + \frac{j_m}{\omega_m}[cos\theta_m - cos(\omega_m t+\theta_m)] + \frac{j_h}{\omega_h}[cos\theta_h - cos(\omega_h t+\theta_h)]\right] \qquad s(t) < x \\ &= 0 \qquad s(t) > x \end{aligned} \tag{8}$$

The time average electric field ($\overline{E}$) at any position x in the sheath can be obtained by integrating *Eq.*(8) over an *rf*-period within limits $\gamma = \pm\omega_l t$ and can be written as

$$\begin{aligned} \overline{E}(x) &= -(d\overline{\varphi}/dx) = (1/2\pi)\int_{-\gamma}^{\gamma} E(x,\omega t)d(\omega t) \\ \Rightarrow &= \left(\frac{e\gamma}{\varepsilon_0\pi}\right)\int_0^x n_i(\varsigma)d\varsigma \\ &\quad -(1/\pi\varepsilon_0\omega_l)\left[j_l(\gamma - sin\gamma) + (j_m/\alpha^2)(\alpha\gamma - sin\alpha\gamma)cos\theta_m + (j_h/\beta^2)(\beta\gamma - sin\beta\gamma)cos\theta_h\right] \end{aligned} \tag{9}$$

Using *Eq.*(9) in limiting conditions *viz.* $x = s$ and $\omega t = \gamma$ at any particular x in the sheath region, one obtains

$$\overline{E}(x) = -\left(\frac{d\overline{\varphi}}{dx}\right) = \left(\frac{j_l}{\pi\varepsilon_0\omega_l}\right)\Bigg[(sin\gamma - \gamma cos\gamma) + \left(\frac{c_{ml}}{\alpha^2}\right)[cos\theta_m sin\alpha\gamma - \alpha\gamma cos(\alpha\gamma+\theta_m)]$$

$$+\left(\frac{c_{hl}}{\beta^2}\right)[cos\theta_h sin\beta\gamma - \beta\gamma cos(\beta\gamma+\theta_h)]\Bigg] = \left(\frac{j_l}{\pi\varepsilon_0\omega_l}\right)g_o \qquad (10)$$

Inserting the mean ion density (Eq.6) into sheath dynamics equation (Eq.7), *with* $x = s$ and $\omega t = \gamma$, one thus obtains

$$\left(1-\frac{2\bar{\varphi}}{T_e}\right)^{1/2}\left(\frac{d\gamma}{dx}\right) = (1/s_o)\left[sin\gamma + c_{ml}sin(\alpha\gamma+\theta_m) + c_{hl}sin(\beta\gamma+\theta_h)\right]^{-1} = (1/s_o f_o), \qquad (11)$$

with $s_o(= j_l / n_0 e\omega_l)$. The set of equations *viz. Eqs.*(10-11) yields a self-consistent description of the *RF* sheath and phase evolution. Combining Eqs.(10 & 11) and integrating with appropriate boundary conditions *viz.* $\bar{\varphi} = 0 \ at \ \gamma = 0$, one can easily be solved to get the time averaged potential structure, as follows

$$\frac{d\bar{\varphi}}{(1-2\bar{\varphi}/T_e)^{1/2}} = -\left(\frac{s_o j_l}{\pi\varepsilon_0\omega_l}\right)f_o g_0 d\gamma \Rightarrow \left(1-\frac{2\bar{\varphi}}{T_e}\right)^{1/2} = 1 + H\int f_o g_0 d\gamma, \qquad (12)$$

where $H(= s_o^2 / \pi\lambda_d^2)$ and $\lambda_d[= (\varepsilon_0 T_e / en_0)^{1/2}]$ is the *Debye* length. This equation also refers to the ion density and can be expressed by using it (*Eq.*12) with Eq.(6) as follows

$$n_i(x) = n_0\left(1-\frac{2\bar{\varphi}}{T_e}\right)^{-1/2} = n_0\left[1 + H\int f_o g_0 d\gamma\right]^{-1}, \qquad (13)$$

Substituting for $\bar{\varphi}$ from *Eq.*(12) in *Eq.*(11) and integrating it again with initial boundary conditions $\gamma = 0 \ at \ x = 0$, one can write

$$(x/s_o) = \int f_o\left[1 + H\int f_o g_0 d\gamma\right]d\gamma. \qquad (14)$$

The above set of derived equations (*Eqs.*10-14) describes the time averaged sheath evolution of the discharge parameters self-consistently and can be solved numerically for any particular case/ choice of parameters. It is also verified that the present analysis is consistent with available analytical expression for fundamental sinusoidal signal by putting $j_m = j_h = 0$. The oscillatory motion of the sheath invokes the potential and field structures which eventually characterizes *iedf.* The consistent nonlinear evolution of the sheath motion and discharge parameters *viz.* corresponding mean electric field ($\bar{E}$) and mean electric potential ($\bar{\varphi}$), corresponding to triple frequency setup has been illustrated as a function of phase (γ).

The plasma electrons interacting with oscillating electron sheath lose energy in its collapsing phase while some of the electrons gain energy in the expanding sheath; effectively in an *rf*-period electrons gain a finite energy. However, in literature, the presence of field reversal during the collapsing phase of sheath (for hydrogen, neon and electronegative plasmas) has been reported, which may contribute the additional electron heating[68-74]. This effect is ignored in the present analysis. Using kinetic approach for current driven mode in case of single frequency discharge this average energy gain by electrons in the collisionless regime has been estimated by *Lieberman*[35]. Following the approach similar to that of *Lieberman*[35] the sheath heating can be written as

$$S_L = m_e u_e \left\langle (u_s - \upsilon_o) n_s u_s \right\rangle_\gamma \Rightarrow m_e u_e j_l \left\langle (u_s - \upsilon_o) f_o \right\rangle_\gamma , \tag{15}$$

where $u_s = (ds/dt) = u_o f_o \left[1 + H \int f_o g_o d\gamma \right]$ is the instant sheath edge velocity, $\upsilon_o (= u_o f_o)$ refers to the time varying oscillatory velocity of the electrons (at ion sheath edge) under influence of applied *rf* current with $u_o = (j_l / n_0)$. This refers to $(u_s - \upsilon_o) \sim u_o f_o H \int f_o g_o d\gamma$ and *Eq.*(15) can be written as

$$S_L = m_e n_o u_e u_o^2 \left\langle f_o^2 H \int f_o g_o d\gamma \right\rangle = S_o \left\langle f_o^2 H \int f_o g_o d\gamma \right\rangle_\gamma , \tag{16}$$

However, this estimate for sheath heating by *Lieberman*[35] treatment ignores the influence of applied electric field on bulk electrons. This assumption violates the current conservation condition at the electron sheath edge[20, 24]. This fact was taken into account by *Kaganovich et al.*[40] in their analysis and the formulation established that *Lieberman* expression overestimates the sheath heating for low *H* values in case of *sf* current profile. Following the *Kaganovich* kinetic treatment the modified expression for sheath heating can be written as follows

$$S_K = m_e n_o u_e u_o^2 \left\langle (u_s - \upsilon_o)^2 (n_i / n_0) \right\rangle_\gamma = S_o \left\langle f_o^2 H^2 \left[\int f_o g_o d\gamma \right]^2 \left[1 + H \int f_o g_o d\gamma \right]^{-1} \right\rangle_\gamma \tag{17}$$

It is also verified that the electron sheath heating expressions (*i.e. Eqs.*16-17) with $j_m = j_h = 0$, readily reduces to the known expressions for the fundamental *sf* sinusoidal signal, derived in the previous analyses[35,40-41]. It is also verified that the electron sheath heating given by *Kaganovich* formulation, approaches asymptotically at higher **H** to the *Lieberman* estimate.

3. *Simulation scheme and parameters*

We have simulated the current driven triple frequency discharge by using 1D3V electrostatic PIC code for argon plasma in low pressure regime where the discharge is primarily sustained by sheath heating of electrons. The code has been developed by the group of Prof. Miles Turner at *Dublin City University* and has been utilized in numerous recent studies[75-79]; a detailed description about the simulation approach can be seen in *references* [45-46]. The simulation takes account of all the possible interaction processes between the particles (*viz.* elastic/ inelastic/ charge exchange/ ionization) via manifesting the Particle-in-Cell (PIC)[45-46] and Monte Carlo collision (MCC)[47-48] schemes together; this have been utilized to estimate the self-consistent plasma discharge features. The accuracy, stability and resolution of the simulation has been taken care of by appropriate choice of step size of time and space which is taken to be smaller than the plasma frequency and Debye length. The discharge system composed of mutually parallel coupled electrodes of infinite dimension which can be operated both *viz.* current and voltage driven modes; in this particular analysis we have used it in current driven mode. In order to simulate the present analysis the electrode gap of 5*cm* filled with argon (*Ar*) gas at low pressure

($5mTorr$) has been considered. In order to compare the simulation results with the analytical treatment, the boundary walls (electrodes) are considered perfectly absorptive for the plasma particles and the secondary electron emission from the electrodes are ignored. The simulation has been carried out for the following standard set of the discharge plasma parameters and effect of individual parameter has been examined keeping others constant.

$j_l = 4A/m^2, j_m = 20A/m^2, j_h = 40A/m^2$, $f_l = 2MHz, f_m = 16MHz, f_h = 80MHz$, $\varphi_l = \varphi_m = \varphi_h = 0$, $c_{ml} = 5, c_{hl} = 10$, $\alpha = 8, \beta = 40$, $T_{eo} = 17406K$, $T_{io} = T_g = 300K$ and $p_g \approx 5mTorr$; T_{eo} and $T_{io}(T_g)$ are initial electron and ion (gas) temperature while p_g refers gas pressure. Here we vary middle frequency *i.e.* f_m and keep other simulation parameters constant.

A train of current driven pulse (as given in Eq.1) has been applied for longer period of time in order to achieve the steady state plasma discharge and the numerous plasma parameters in an *rf*-cycle has been displayed as outcome. We have evaluated the electron sheath heating and *iedf* of the discharge in triple frequency current driven mode, in-particular, the effect of intermediate frequency (f_m) component on numerous physical parameters, keeping rest the parameters same and the results are discussed in the next section.

4. *Numerical results and discussion*

It is well understood that the applied *rf*-source over the electrode causes an instantaneous oscillatory electric field response to the plasma electrons, prominently in the proximity of the electrodes. The applied field significantly diminishes within few Debye scale lengths while moving from the electrodes to the centre of discharge (*i.e.* sheath region (as $E_x \propto e^{-x/\lambda_d}$)). A much weaker electric field exists inside the bulk or pre-sheath region and the plasma density self-consistently decays from centre of discharge to electrodes. In general, in an *RF* cycle the electrons interacting with expanding sheath get kicks and depending on interaction of the phase with the electron sheath edge, electrons either gain or lose energy. On the other hand, electrons lose its energy during collapsing phase of the sheath. However over an RF cycle there is a net gain in electron energy. When multiple frequency signals are applied to the electrodes, the instantaneous movement of electrons depend on the superposition of constituent current signals; in particular to the resulting electric field, whose amplitude, following Maxwell equations, varies proportional to the current magnitude and inversely proportional to the frequency component (*i.e.* $E_{rf} \propto j_{rf} / f_{rf}$). For the instance if one chose the peak current in all three cases viz. *sf*, *df and tf modes* constant, the sheath features are sensitive to the choice of the frequencies. It is well understood and stated before, that in *df-CCP* discharge, lower and higher frequency components control the features of *iedf* and plasma ionization respectively; the inclusion of intermediate frequency intuitively stimulate that particular aspect which is closer to it, due to significant mutual frequency overlap. For example, one should anticipate large sheath potential drop (additional control over *iedf*) in case of $f_m \to f_l$ while larger plasma density as $f_m \to f_h$. This characteristic also replicates in collisionless sheath heating with multiple signals where it is anticipated to decrease with increasing the higher frequency components[23]. First we illustrate the numerical results for the sheath parameters and electron sheath heating, corresponding to analytical formulation made in *Section*-2. The simulation results based on PIC has been discussed in the consequent subsection.

Numerical results with analytical formulation

The set of Fig.2 demonstrates the steady state self-consistent nonlinear discharge evolution as a function of phase (γ) by the inclusion of higher frequency component. The computations correspond to standard set of parameters mentioned in *Section*-3. Fig.2a reflects the current form in the three cases *viz.* when the discharge is operated in *sf, df and tf* mode. As anticipated the powered electrode is driven by superposition of multiple current signals. The sheath oscillation (span, *x*) and corresponding evolution of the mean sheath potential ($\bar{\varphi}$) in the expanding phase (*i.e.* $0 \le \gamma \le \pi$) of the oscillation, have been illustrated in Figs.2b and 2c respectively. Symmetrical behaviour is anticipated in collapsing phase *i.e.* $\pi \le \gamma \le 2\pi$. The sheath span (*x*) and mean sheath potential ($\bar{\varphi}$) is seen to be larger in *tf* driven discharge than that in case of *sf* mode for the chosen set of data; the $\bar{\varphi}$ variation also reciprocate the evolution of the mean electric field ($\bar{E}$). The collisionless capacitive electron sheath heating based on *Kaganovich* formulation in these three different operating modes has been displayed in Fig.3a as a function of the parameter *H*. The sheath heating is seen to be largest in case of *tf* operating mode. This is primarily a consequence of large mean sheath potential (Fig.2c). The *Kaganovich* formulation is noticed to approach *Lieberman* estimate with the inclusion of additional frequency components and increasing values of parameter *H*; this nature has been showed in Fig.3b for the given set of parameters. Next to this, we consider the case of *tf* operated mode for our further computation and try to explore the role of middle frequency component in CCP discharge.

The evolution (*x*) of electron sheath by varying the middle frequency in *tf* discharge configuration has been illustrated in Fig.4a and as anticipated, the span is noticed to increase as the middle frequency approaches to lower frequency (~2*MHz*). Corresponding variation of f_m on the discharge sheath potential has been displayed in Fig.4b. It is found that sheath potential fluctuate at higher magnitude as f_m approaches to lower frequency f_l. In particular, the analytically calculated sheath potential drop significantly at $f_m \sim 40MHz$ compared to $\sim 16MHz$ (Fig.4b). This average sheath potential physically determine the *ion energy distribution function* (*iedf*), responsible for etching and film deposition in material processing using *CCP* discharges. The decrease in the sheath potential with increasing f_m

may cause the absence of high energy ions and possess low energy particles in the proximity of electrode. The mean energy gained (*Kaganovich* estimate) by electrons due to oscillatory sheath in collisionless regime has been displayed in Fig.4c and follows trend similar to Figs.(4a-b) as the heating is noticed to increase as $f_m \rightarrow f_l$. This nature can be attributed to the effects due to appropriate superposition and weaker destructive interference between the frequency components of applied current signals, as intermediate frequency approaches the lowest frequency.

PIC results for CCP discharge with tf configuration

The PIC simulation has been conducted using 1D3V electrostatic code for the set of data given in *Section*-3 and the role of middle frequency component in *tf* configuration has been explored. In simulation results, the powered electrode is located at 0 *cm* and grounded electrode is at 5 *cm*.The time averaged electron (dashed line) and ion (solid line) density profile in the steady state of the plasma discharge has been illustrated in Fig.5. The peak density in the curve shows a pecular phenomenon in that it rises and falls as the middle frequency is increased. On the other hand the total number of ions in the discharge seem to monotonically go up with the increase of the middle frequency f_m. This may be attributed to an optimization in the number of the electrons/ ions in the discharge volume for a particular intermediate frequency (f_m ~20*MHz*). The increase of electrons/ ions in the discharge volume with increasing f_m is primarily due to enhancement of effective modulated frequency in *tf* mode. As a consequence the sheath width (span) is discerned to decrease and is in qualitative agreement with the analytical assessment (*Fig*.4a). This can be understood in terms of increase in plasma shielding with increasing density. Theory predict the average sheath span (in *cm*) of ~1.78, 1.51, 1.34, 1.24 and 0.79 for $f_m = 8MHz$, 10*MHz*, 16*MHz*, 20*MHz* and 40*MHz* respectively which is in reasonable agreement with the *PIC* results (verified from density profile in Fig.5). The axial profile of mean plasma potential of the discharge has been displayed in Fig.6 where it is seen to be large when the middle frequency f_m is close to lower frequency. This fact is also consistent with our analytical prediction (Fig.4b). The effect of f_m on *iedf* at the powered electrode (0 *cm*) is primarily governed by potential drop over the sheath and has been described in Fig.7. It is noticed that the presence of high energy ions decreases as f_m approaches to the high frequency component. At $f_m = 40MHz$ the energy of ions are significantly reduced (~300 *eV*) compared to $f_m = 08MHz$ (~800 *eV*). This may be attributed to decrease in the sheath potential with increasing f_m and consequently a control over the production of highly energetic ions.

In collisionless case, as a consequence of the sheath oscillation, the interacting electrons in collapsing and expanding phase effectively gain a finite positive energy in an rf-cycle. This results in the collisionless heating of electrons in the vicinity of sheath. The spatiotemporal profile of the electric field and the sheath heating for $f_m = 8MHz$, 20*MHz* and 40*MHz* has been displayed in Fig.8 for last two rf cycles. The interplay of sheath dynamics and its consequent increase in sheath heating by reducing the middle frequency is clearly visible in this figure. The time averaged electron sheath heating corresponding to different values of f_m has been shown in Fig.9. In this discharge profile, the collisionless electron sheath heating peaks at some point in the proximity of the sheath edge; this can be understood in terms of mutual competitive phenomena of decreasing local electric field and increasing plasma density ($J.E \propto n_e E^2$) in sheath. The electron sheath heating is seen to acquire double peaks at smaller f_m values; this may correspond to the peaks occurring in the sheath potential (Fig.4) in an RF cycle which drives the electron heating effectively in the sheath. It should be noted that the net heating (S_{stoc}) is composed of contributions from both *viz.* applied *RF* (S_{rf}) current signal and the *dc* sheath part S_{dc} (*i.e. floating sheath*). The *dc* floating sheath eventually refers to the negative heating (S_{dc}) in the proximity of the electrode which means the plasma near the electrode becomes colder. In simulation, the *rf* electron sheath heating (S_{rf}) has been obtained by dropping the *dc* contribution (S_{dc}) from the net collisionless heating (S_{sh}). An estimate of the time average (averaged over 100 RF cycles) sheath heating of the electrons ($S_{rf} = S_{sh} - S_{dc}$) using PIC simulation operating in *tf* mode for different f_m has been depicted in Fig.10 (solid blue dots with line). It clearly demonstrates that the sheath heating is sensitive to the frequency ratios (*i.e.* f_m) in *tf*-mode of discharge operation. The points refer to the analytical prediction of the electron sheath heating as a function of f_m corresponding to the data set used for PIC simulation; *red* (*triangle*) and *black* (*square*) solid points refer to *Lieberman* (S_L, *Eq.*16) and *Kaganovich* (S_K, *Eq.*17) estimates respectively. The PIC estimates are observed to be in reasonable agreement with *Kaganovich* formulation. The analytical (*Figs.*3-4) and the PIC simulation (Figs.6-8) estimates reveal an important feature that the sheath dynamics, ion energy and electron sheath heating can be controlled by scaling the intermediate frequency in *tf-configuration* of *CCP* discharge. Further it should be noted that the outcomes of the analysis are strictly relevant to the ~~systems~~ operating in collisionless regime.

5. *Summary*

In summary, an analytical model (based on *sf* sheath modelling given by *Lieberman*[35] and *Kaganovich et al*[40]) for stochastic heating in *tf* current driven CCP discharge has been developed. It is observed that the stochastic heating is dependent on the intermediate frequency of applied RF signal. The heating estimated by analytical model has been further verified with help of 1D3V electrostatic PIC code and found in reasonable agreement with simulation results. It is also observed that the *ion energy distribution function* (*iedf*) at the electrode can be controlled by tuning the intermediate frequency. The maximum energy of ions arriving at the electrodes reduces when the middle frequency approaches the higher frequency. This is because the potential across sheath is modified by tuning the middle frequency. It allows a control over power deposition at the electrode in *CCP* discharges. This is of relevance to the etching/ deposition processes in numerous material processing applications in micro-nano fabrications.

Acknowledgments

This work is supported by Department of Science & Technology (*DST*), *Government of India via Projects GITA/ DST/ TWN/ P*-56/ 2014, *DST-JC Bose Fellowship and YOS Professor PKK* 92-14.

References

1. M. Lieberman and A. J. Lichtenberg, *Principles of Plasma Discharges and Materials Processing* (Wiley: NJ, 2005).
2. B. G. Heil, U. Czarnetzki, R. P. Brinkmann and T. Mussenbrock, *J. Phys. D: Appl. Phys.* **41**(16) 165202 (2008).
3. J. Schulze, E. Schungel and U. Czarnetzki, *J. Phys. D: Appl. Phys.* 42, 092005 (2009).
4. J. Schulze, E. Schungel, Z. Donko and U. Czarnetzki, *Plasma Sources Sci. Technol.* 20, 015017 (2011).
5. Z. Donko, J. Schulze, P. Hartmann, I. Korolev, U. Czarnetzki and E. Schungel, *Appl. Phys. Lett.* 97, 081501 (2010).
6. E. Schungel, J. Schulze, Z. Donko and U. Czarnetzki, *Phys. Plasmas* 18, 013502 (2011); *D: Appl. Phys.* 41, 165202 (2008).
7. Z. Donko, *Plasma Sources Sci. Technol.* 20, 024001 (2011).
8. Lafleur T. and Booth J. P. 2012, *J. Phys. D: Appl. Phys.* 45, 395203.
9. D. J. Coumou, D. H. Clark, T. Kummerer, M. Hopkins, D. Sullivan and S. Shannon, *IEEE Trans. Plasma Sci.* 42, 1880 (2014).
10. A. C. F. Wu, M. A. Lieberman and J. P. Verboncoeur, *J. Appl. Phys.* 101, 056105 (2007).
11. M. Olevanov, O. Proshina, T. Rakhimova and D. Voloshin, *Phys. Rev. E* 78, 026404 (2008).
12. W. C. Chen, X. M. Zhu, S. Zhang and Y. K. Pu, *Appl. Phys. Lett.* 94, 211503 (2009).
13. D Israel and K-U Riemann, *J. Appl. Phys.* 99, 093303 (2006).
14. J. K. Lee, O. V. Manuilenko, N. Yu Babaeva, H. C. Kim and J. W. Shon, *Plasma Sources Sci. Technol.* 14, 89 (2005).
15. Z. Zhou, R. Linghu, M. Deng and D. Xiong, *Jour. Appl. Phys.* 112, 063306 (2012).
16. T. Lafleur, R. W. Boswell and J. P. Booth, *Appl. Phys. Lett.* **100,** 194101 (2012).
17. T. V. Rakhimova, O. V. Braginsky, V. V. Ivanov, A. S. Kovalev, D. V. Lopaev, Y. A. Mankelevich, M. A. Olevanov, O. V. Proshina, A. T. Rakhimov, A. N. Vasilieva and D. G. Voloshin, *IEEE Trans. Plasma Sci.* 35, 1229 (2007).
18. T. Lafleur, P. A. Delattre, E. Johnson and J. P Booth, *Appl. Phys. Lett.* 101, 124104 (2012).
19. P. A. Delattre, T. Lafleur, E. Johnson and J. P. Booth, *J. Phys. D: Appl. Phys.* 46, 235201 (2013).
20. H. H. Goto, H. D. Lowe and T. Ohmi, *J. Vac. Sci. & Tech. A* 10, 3048 (1992).
21. H. H. Goto, H. D. Lowe and T. Ohmi, , *IEEE Trans. Semicond. Man.* 6, 58 (1993).
22. V. Georgieva and A. Bogaerts, *J. Appl. Phys.* 98 023308 (2005)
23. S Sharma, S K Mishra, P K Kaw, A Das, N Sirse and M. M. Turner, *Plasma Sources Sci. Technol. Sour.* 24, 025037 (2015).
24. M. M. Patterson, H.Y. Chu and A. E. Wendt, *Plasma Sources Sci. Technol.* **16**, 257 (2007).
25. T. Baloniak, R. Reuter and A. von Keudell, *J. Phys. D: Appl. Phys.* 43, 335201 (2010)
26. E. Schüngel, Z. Donkó, P. Hartmann, A. Derzsi, I. Korolov and J. Schulze, *Plasma Sources Sci. Technol.* **24**, 045013 (2015).
27. T. Lafluer, *Plasma Sources Sci. Technol.* **25**, 013001 (2015).
28. H. C. Kim, J. K. Lee and J. W. Shon, *Phys. Plasmas* 10, 4545 (2003).
29. C. F. Alan Wu, M. A. Lieberman and J. P. Verboncoeur, *J. Appl. Phys.* 101 056105 (2007).
30. H. C. Kim and J. K. Lee *Phys. Rev. Lett.* 93, 085003 (2004).

31. H. C. Kim, F. Iza, S. S. Yang, m. Radmilovic-Radjenovic and J. K. Lee, *J. Phys. D: Appl. Phys*. 36 R, 283 (2005).
32. G. Y. Park, S. J. You, F. Iza and J. K. Lee, *Phys. Rev. Lett.* 98, 085003 (2007)
33. S. H. Lee, P. K. Tiwari, J. K. Lee, *Plasma Sources Sci. Technol. Sour.* 18, 025024 (2009).
34. Rahman M. T. and Dewan M. N. A. 2015, *Plasma Sci. Tech.* 17, 141
35. M. A. Lieberman, *IEEE Trans. Plasma Sci*. 16, 638 (1988).
36. S. Sharma, "*Investigation of Ion and Electron Kinetic Phenomena in Capacitively Coupled Radio-Frequency Plasma Sheaths: A Simulation Study*" Ph.D thesis, *Dublin City University* (2013).
37. O. A. Popov and V. A. Godyak, *J. Appl. Phys.* 57, 53 (1985).
38. V. A. Godyak and R. B. Piejak, *Phys. Rev. Lett.* 65, 996 (1990).
39. I. D. Kaganovich, V. I. Kolobov and L. D. Tsendin, *Appl. Phys. Lett.* **69**, 3818 (1996).
40. I. D. Kaganovich, O. V. Polomarov and C. E. Theodosiou, *IEEE Trans. Plasma Sci.* **34**, 696 (2006).
41. E. Kawamura, M.A. Lieberman and A. J. Lichtenberg, *Phys. Plasmas* **13**, 053506 (2006).
42. S. Sharma and M. M. Turner, *J. Phys. D: Appl. Phys.* **46**, 285203 (2013).
43. S. Sharma, S. K. Mishra and P. K. Kaw, *Phys. Plasmas* 21, 073511 (2014).
44. S. Sharma, S. K. Mishra, P. K. Kaw, M. M. Turner and S. K. Karkari, *Contrib. Plasma Phys*. 55 (4), 331 (2015).
45. J. P. Verboncoeur, *Plasma Phys. Control. Fusion* 47, A231 (2005)
46. M. M. Turner, A. Derzsi, Z. Donkó, D. Eremin, and S. J. Kelly, *Phys. Plasmas* 20, 013507 (2013).
47. C. K. Birdsall, *IEEE Trans. on Plasma Sci.* **19** 65 (1991).
48. R. W. Hockney and J. W. Eastwood, *Computer simulation using particles* (Adam Hilger: Bristol, 1988).
49. S. Sharma and M. M. Turner, *Plasma Sources Sci. Technol.* **22**(3), 035014 (2013).
50. S. Sharma and M. M. Turner, *Phys. Plasmas* **20** 073507 (2013).
51. J. Schulze, B. G. Heil, D. Luggenh¨olscher, R. P. Brinkmann and U. Czarnetzki, *J. Phys. D: Appl. Phys.* **41** 195212 (2008).
52. J. Schulze, B. G. Heil, D. Luggenh¨olscher, T. Mussenbrock, R. P. Brinkmann and U. Czarnetzki, *J. Phys. D: Appl. Phys.* **41** 042003 (2008).
53. B. M. Annaratone, V. P. T. Ku and J. E. Allen, *J. Appl. Phys.* **77** 5455 (1995).
54. V. P. T. Ku, B. M. Annaratone and J. E. Allen, *J. Appl. Phys.* **84** 6536 (1998).
55. W. D. Qiu, K. J. Bowers and C. K. Birdsall, *Plasma Sources Sci. Technol.* **12** 57 (2003).
56. U. Czarnetzki, T. Mussenbrock and R. P. Brinkmann, *Phys. Plasmas* **13** 123503 (2006).
57. T. Mussenbrock and R. P. Brinkmann, *Appl. Phys. Lett.* **88** 151503 (2006).
58. T. Mussenbrock, D. Zeigler and R. P. Brinkmann, *Phys. Plasmas* **13** 083501 (2006).
59. T. Mussenbrock and R. P. Brinkmann, *Plasma Sources Sci. Technol.* **16** 377 (2007).
60. L. Tonks L. *Phys. Rev.* **19** 1458 (1931).
61. L. Tonks, *Phys. Rev.* **38** 1219 (1931).
62. A. Dattner, *Phys. Rev. Lett.* **10** 205 (1963).
63. J. V. Parker, J. C. Nickel and R. W. Gould, *Phys. Fluids* **7** 1489 (1964).
64. J. Taillet, *Am. J. Phys.* **37** 423 (1969).
65. R. P. Brinkmann, *Plasma Sources Sci. Technol.* **24** 064002 (2015).
66. R. P. Brinkmann, *Plasma Sources Sci. Technol.* **25** 014001 (2016).
67. J. Schulze, Z. Donko, A. Derzsi, I. Korolov and E. Schuengel, *Plasma Sources Sci. Technol.* **24** 015019 (2015).
68. D. O'Connell, T. Gans, A. Meige, P. Awakowicz and R. W. Boswell, *IEEE Trans. Plasma Sci.* **36** 1382 (2008).
69. A. Meige, D. O'Connell, T. Gans and R. W. Boswell, *IEEE Trans. Plasma Sci.* **36** 1384 (2008).
70. T. Gans, C. C. Lin, V. Schulz-von der Gathen and H. F. Dobele, *Phys. Rev. A, Gen. Phys.* **67** 012707 (2003).
71. M. M. Turner and M. B. Hopkins, *Phys. Rev. Lett.* **69** 3511 (1992).
72. U. Czarnetzki, D. Luggenholscher and H.F. Dobele, *Plasma Sources Sci. Technol.* **8** 230 (1999).
73. R. A. Gottscho, *Phys. Rev. A, Gen. Phys.* **36** 2233 (1987).
74. A. H. Sato and M. A. Lieberman, *J. Appl. Phys.* **68** 6117 (1990).
75. M. M. Turner, *Plasma Sources Sci. Technol.* **22** 055001 (2013).
76. P. C. Boyle, A. R. Ellingboe and M. M. Turner, *Plasma Sources Sci. Technol.* **13** 493 (2004).
77. J. Convey, S. Kechkar, N. O' Connor, C. Gaman, M. M. Turner and S. Daniels, *Plasma Sources Sci. Technol.* **22** 045004 (2013).
78. L. Lauro-Taroni, M. M. Turner and N. StJ. Braithwaite, *J. Phys. D: Appl. Phys.* **37** 2216 (2004).
79. M. M. Turner, A. W. Hutchinson, R. A. Doyle and M. B. Hopkins, *Physical Review Lett.* **76** 2069 (1996).

Figure captions

Fig.1a: Schematic diagram of low pressure current driven Ar plasma discharge in *tf-mode*.

Fig.1b: Schematic diagram of high voltage single frequency capacitively coupled plasma sheath.

Fig.2a: Time profile of the applied current signal over discharge electrode in *sf, df and tf* mode for standard set of parameters stated in text.

Fig.2b: Normalized position (*x*) of *RF* electron sheath as a function of phase (γ) in different discharge operating *sf, df and tf* mode for standard set of parameters stated in text.

Fig.2c: Corresponding normalized mean electric potential ($\overline{\varphi}$) as a function of phase (γ) in different discharge operating *sf, df and tf* mode for standard set of parameters stated in text.

Fig.3a: Average electron sheath heating (*Kaganovich* estimate) as a function of parameter *H* for the discharge operating in *sf, df and tf* mode for standard set of parameters stated in text.

Fig.3b: The ratio of electron sheath heating estimates based on *Kaganovich* and *Lieberman* formulation as a function of parameter *H* for the discharge operating in *sf, df and tf* mode for standard set of parameters stated in text.

Fig.4a: Normalized position (*x*) of *RF* electron sheath as a function of phase (γ) in the discharge operating *in tf* mode for different values of f_m corresponding to standard set of parameters stated in text.

Fig.4b: Normalized mean electric potential ($\overline{\varphi}$) as a function of phase (γ) in the discharge operating *in tf* mode for different values of f_m corresponding to Fig.4a.

Fig.4c: *Kaganovich* estimate of electron sheath heating (*Kaganovich* estimate) as a function of parameter *H* in the discharge operating *in tf* mode for different values of f_m corresponding to Fig.4a.

Fig.5: Space evolution of the time average plasma density (n_e, n_i) in the discharge operating *in tf* mode for different values of f_m and standard set of parameters stated in text.

Fig.6: Space evolution of the time mean electric potential ($\overline{\varphi}$) in the discharge operating *in tf* mode for different values of f_m corresponding to Fig.5.

Fig.7: Corresponding **i**on energy distribution function (*iedf*) at powered electrode (x=0 *cm*) in *CCP* discharge operating *in tf* mode for different values of f_m corresponding to Fig.5.

Fig.8: Spatio-temporal profile of the electric field (*E*) and corresponding electron sheath heating ($< J.E >$) in the discharge operating *in tf* mode for different of f_m values *viz.* 8*MHz ((A-1),(A-2))*, 20*MHz ((B-1),(B-2))* and 40*MHz ((C-1),(C-2))*.

Fig.9: Space evolution of the time average electron sheath heating ($< J.E >$) in the discharge operating *in tf* mode for different values of f_m corresponding to Fig.5.

Fig.10: Average electron sheath heating (S_{stoc}) as a function of middle frequency component (f_m); the red (triangle) and black (square) dots refer to *Lieberman* and *Kaganovich* estimate while the blue dots with line correspond to PIC results.

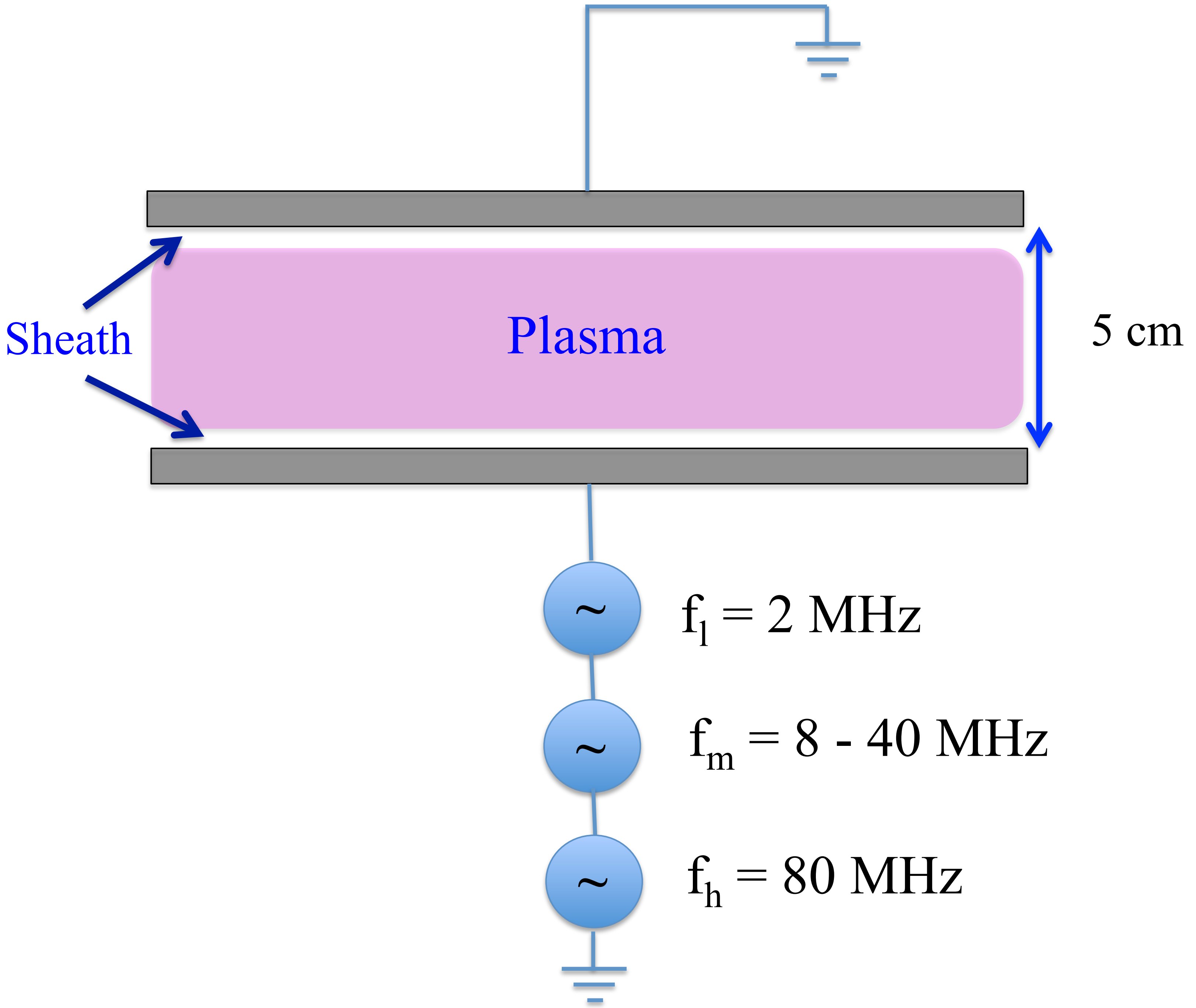
Sheath
Plasma
5 cm
$f_l = 2$ MHz
$f_m = 8 - 40$ MHz
$f_h = 80$ MHz

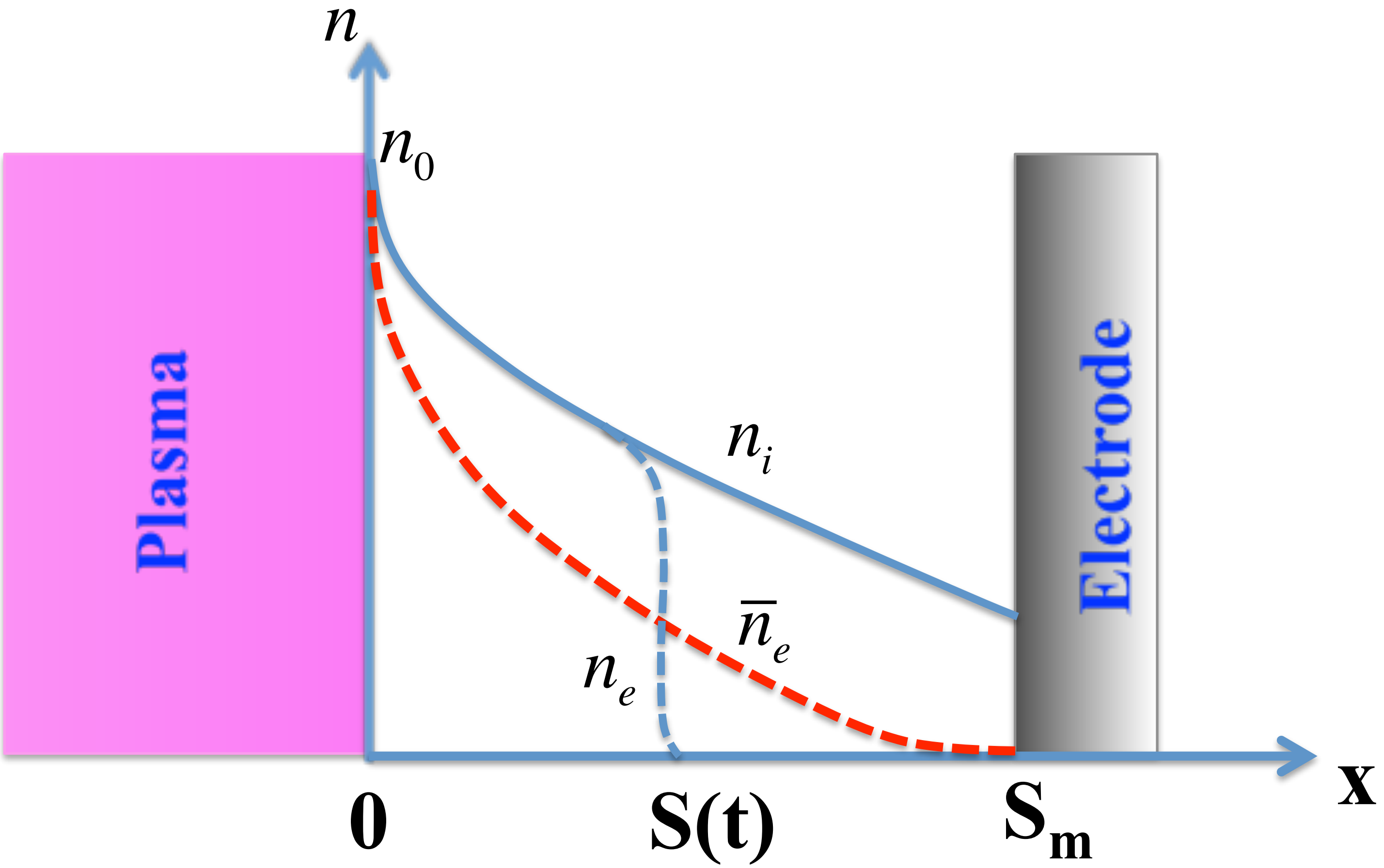
n
n_0
Plasma
n_i
$\overline{n}_e$
n_e
Electrode
0
S(t)
S_m
x

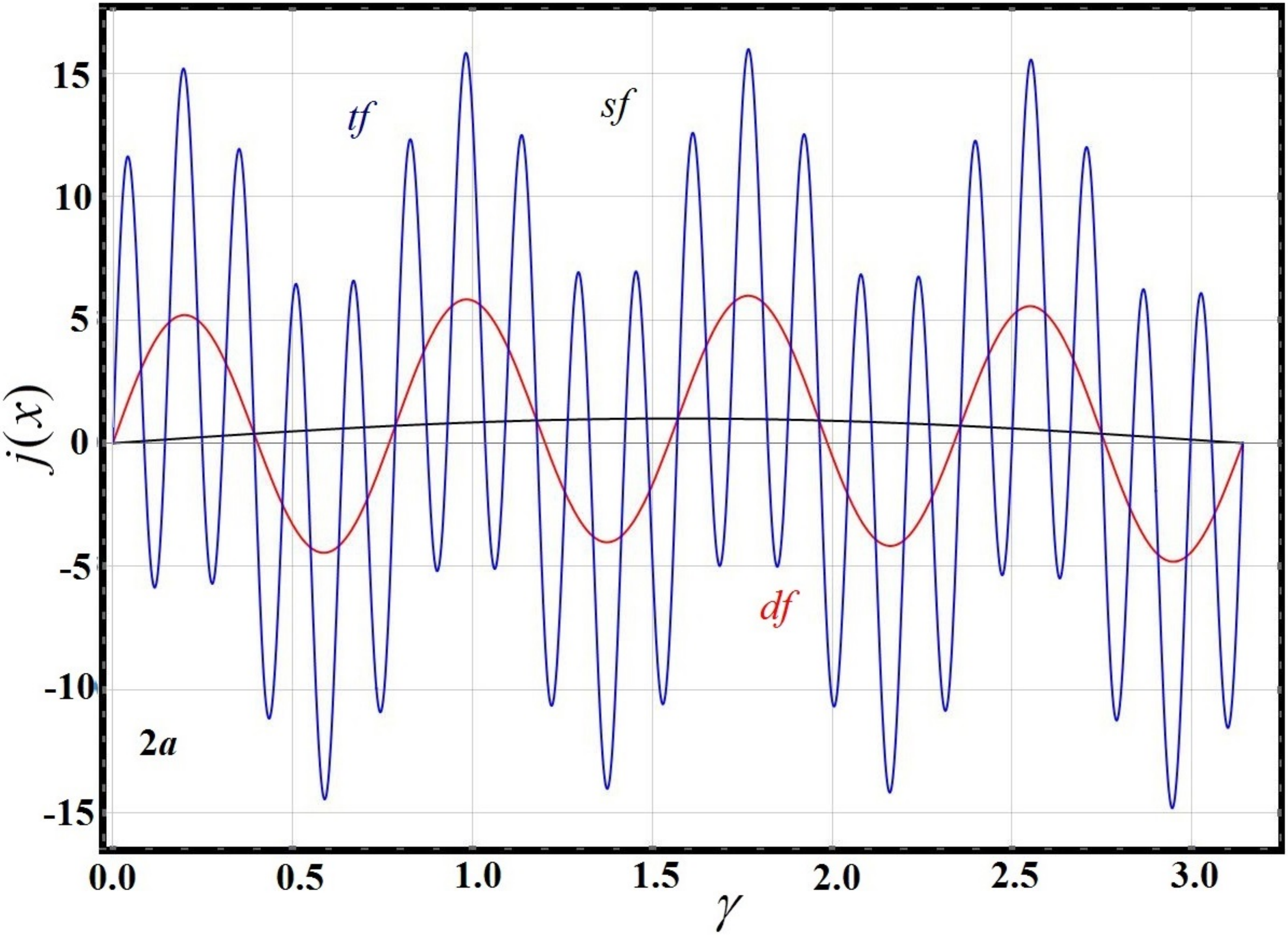
tf
sf
df
2a
15
10
5
0
-5
-10
-15
0.0
0.5
1.0
1.5
2.0
2.5
3.0
$j(x)$
γ

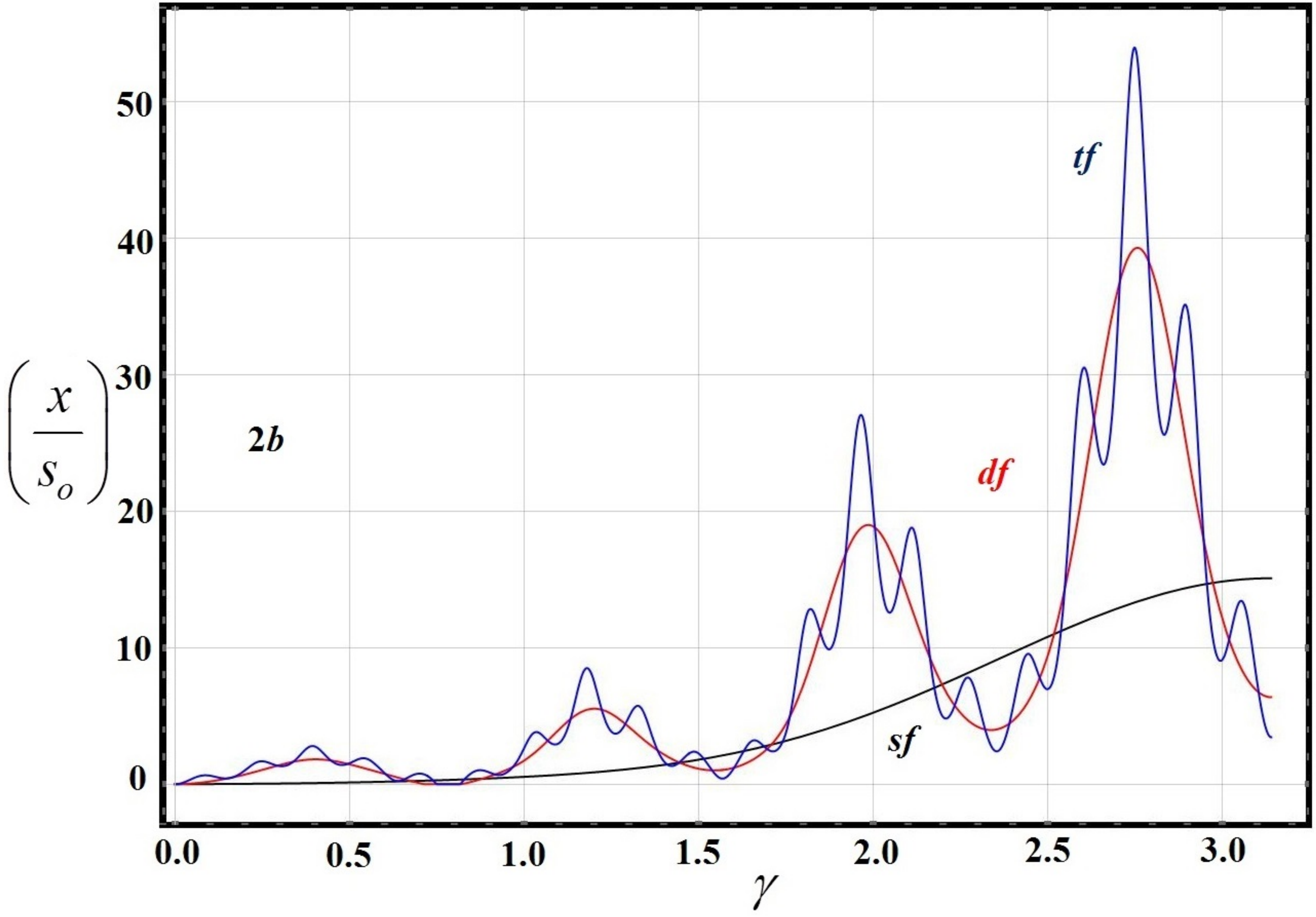

$\left(\frac{x}{s_o}\right)$
2b
tf
df
sf
0
10
20
30
40
50
0.0
0.5
1.0
1.5
2.0
2.5
3.0
γ

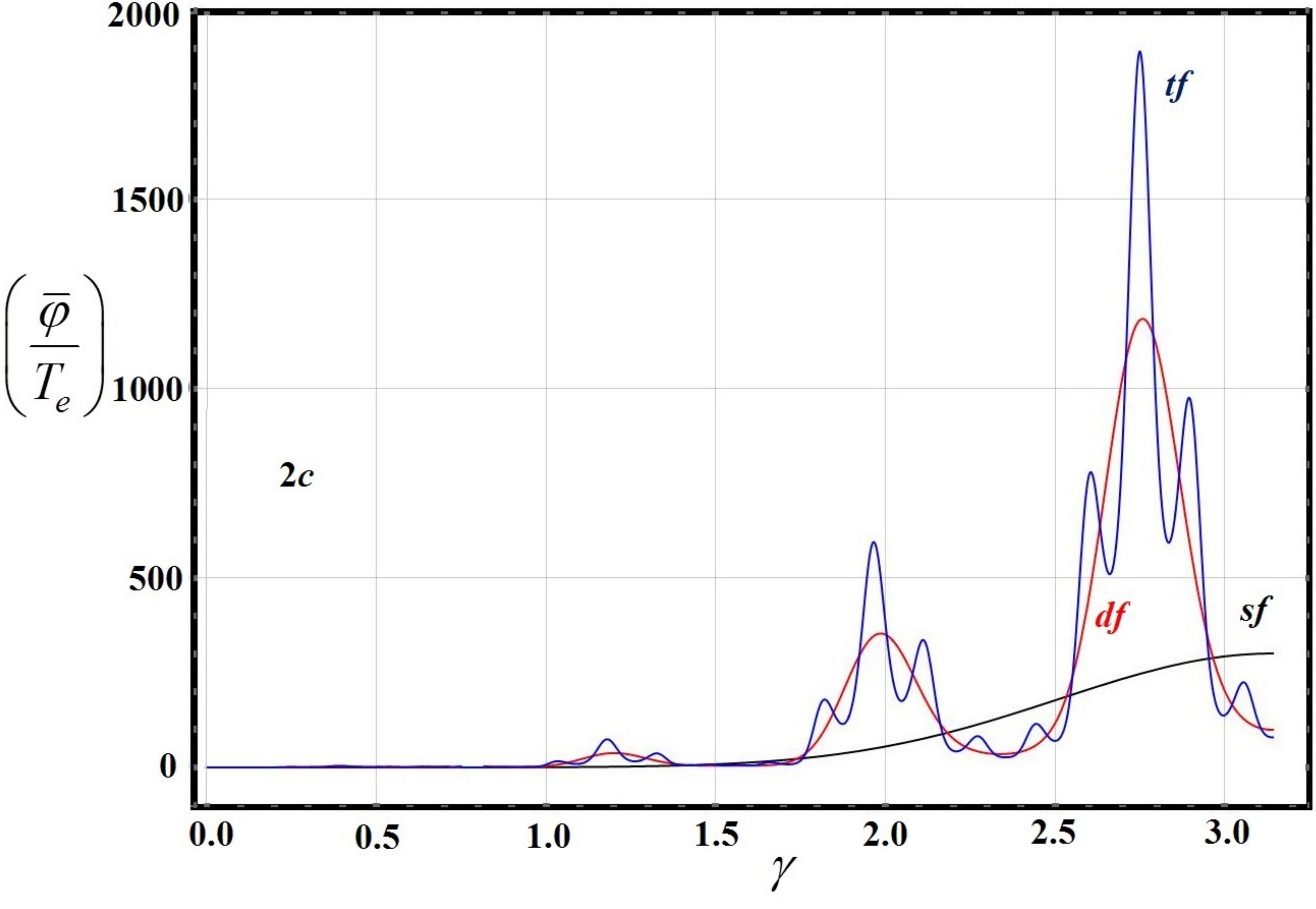
2000
1500
1000
500
0
$\left(\frac{\overline{\varphi}}{T_e}\right)$
2c
tf
df
sf
0.0
0.5
1.0
1.5
2.0
2.5
3.0
γ

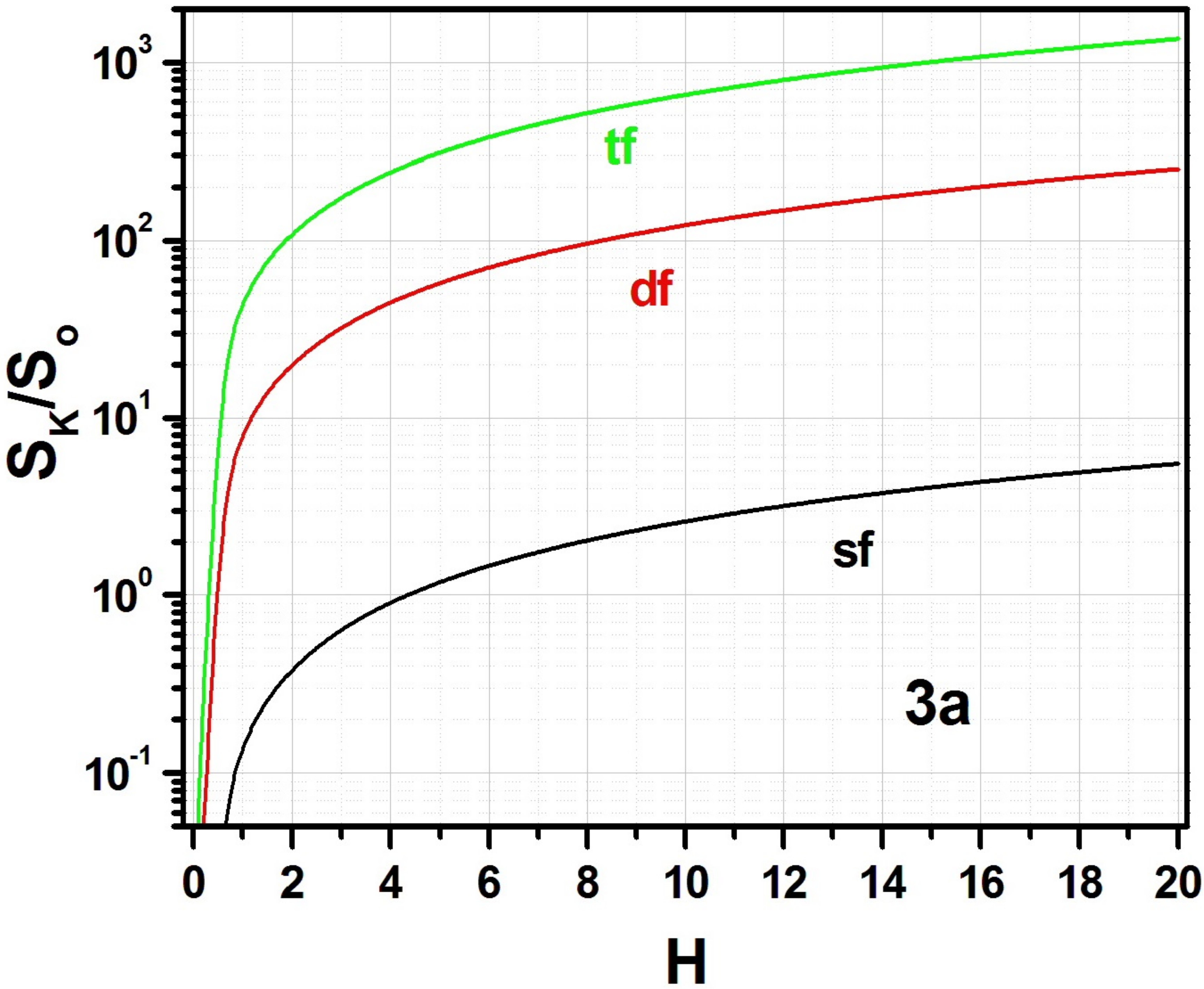
10^3
10^2
10^1
10^0
10^{-1}
S_K/S_o
tf
df
sf
3a
0
2
4
6
8
10
12
14
16
18
20
H

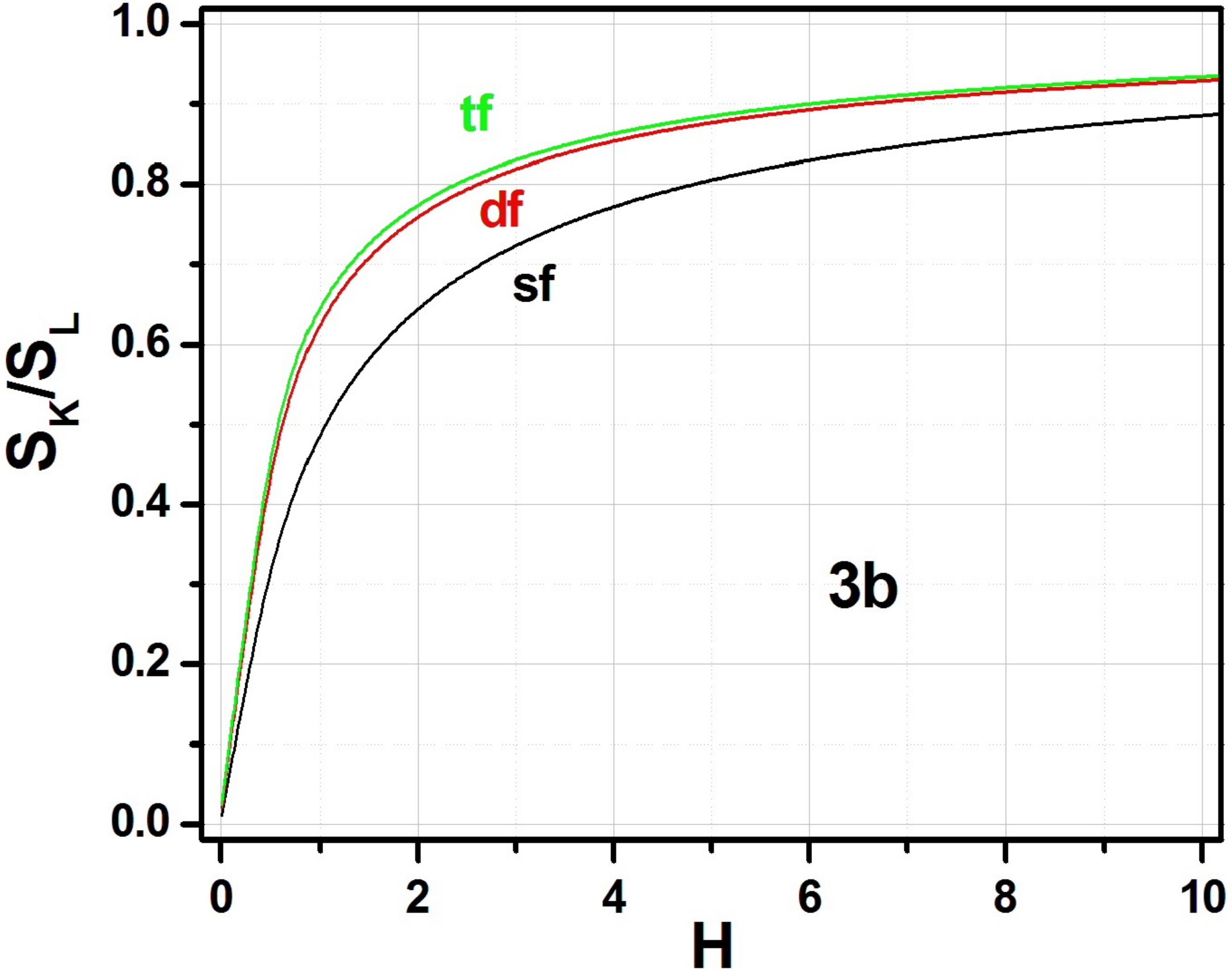

tf
df
sf
3b
S_K/S_L
H
0.0
0.2
0.4
0.6
0.8
1.0
0
2
4
6
8
10

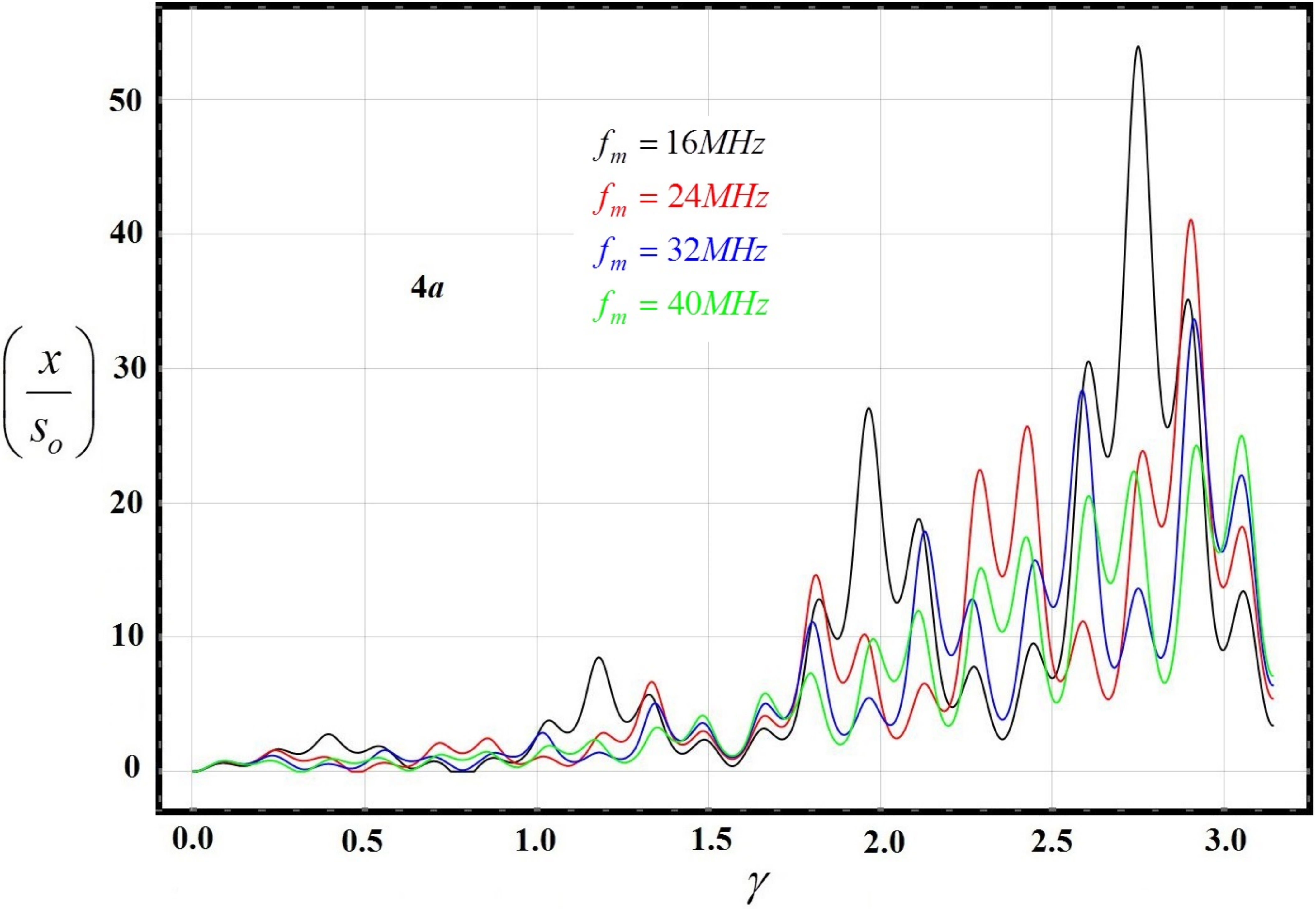
4a
$f_m = 16MHz$
$f_m = 24MHz$
$f_m = 32MHz$
$f_m = 40MHz$
$\left(\frac{x}{s_o}\right)$
50
40
30
20
10
0
0.0
0.5
1.0
1.5
2.0
2.5
3.0
γ

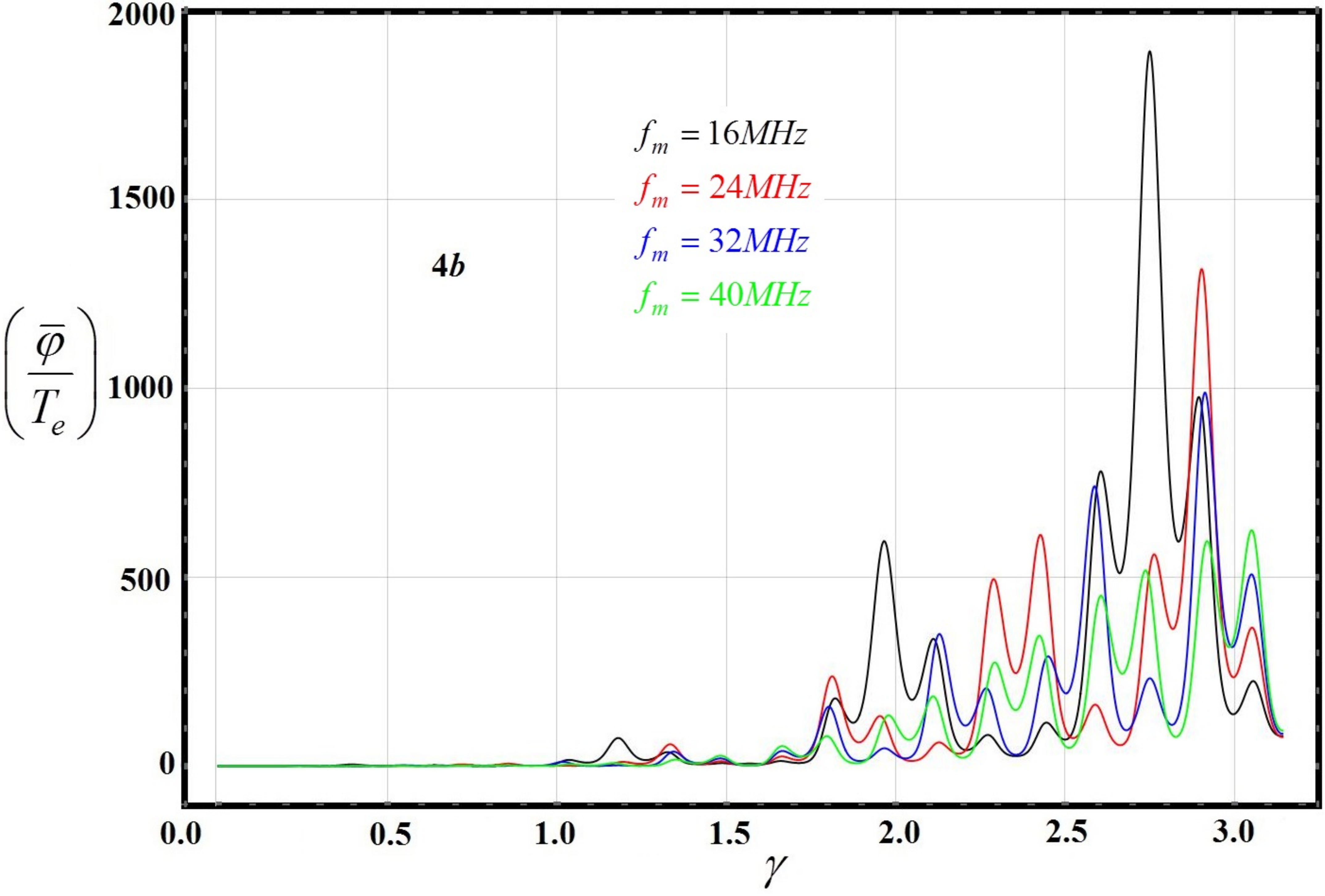
4b
$f_m = 16MHz$
$f_m = 24MHz$
$f_m = 32MHz$
$f_m = 40MHz$
$\left(\frac{\bar{\varphi}}{T_e}\right)$
2000
1500
1000
500
0
0.0
0.5
1.0
1.5
2.0
2.5
3.0
γ

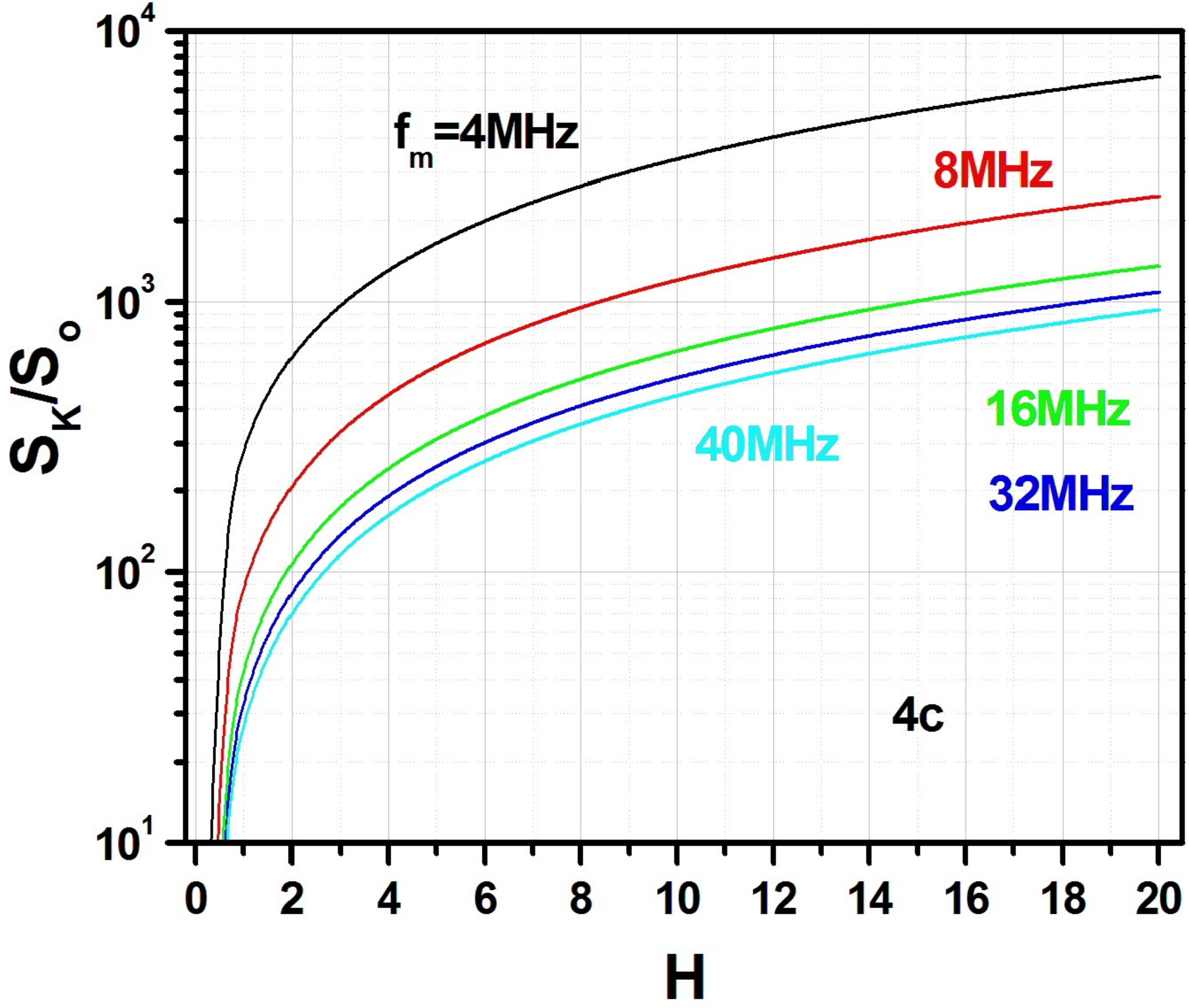

10^4
10^3
10^2
10^1
S_K/S_o
f_m=4MHz
8MHz
16MHz
40MHz
32MHz
4c
0
2
4
6
8
10
12
14
16
18
20
H

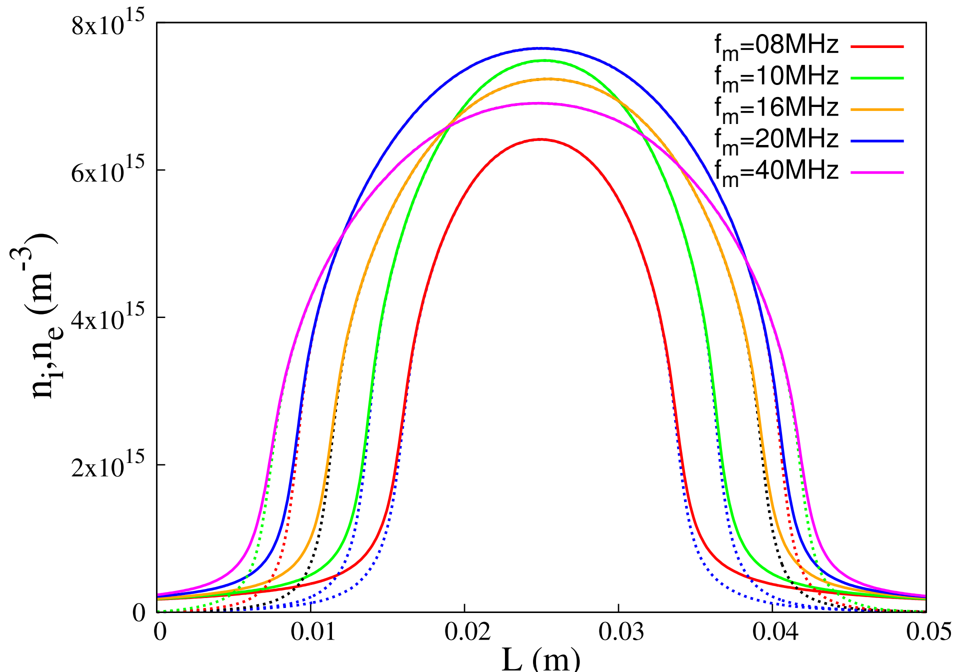
8x10^15
6x10^15
4x10^15
2x10^15
0
0
0.01
0.02
0.03
0.04
0.05
n_i,n_e (m^-3)
L (m)
f_m=08MHz
f_m=10MHz
f_m=16MHz
f_m=20MHz
f_m=40MHz

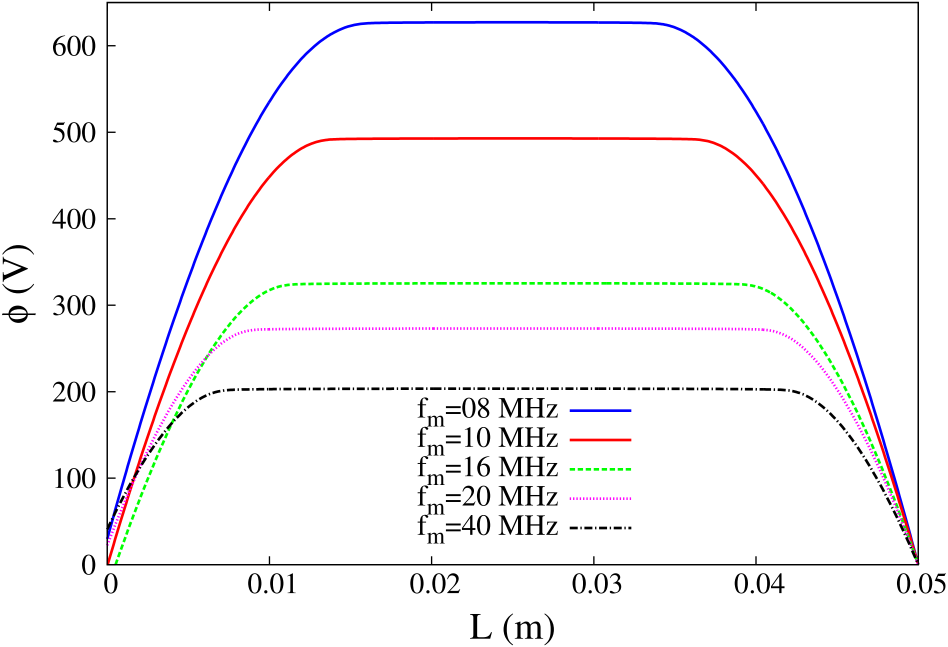

φ (V)
L (m)
0
100
200
300
400
500
600
0
0.01
0.02
0.03
0.04
0.05
f_m=08 MHz
f_m=10 MHz
f_m=16 MHz
f_m=20 MHz
f_m=40 MHz

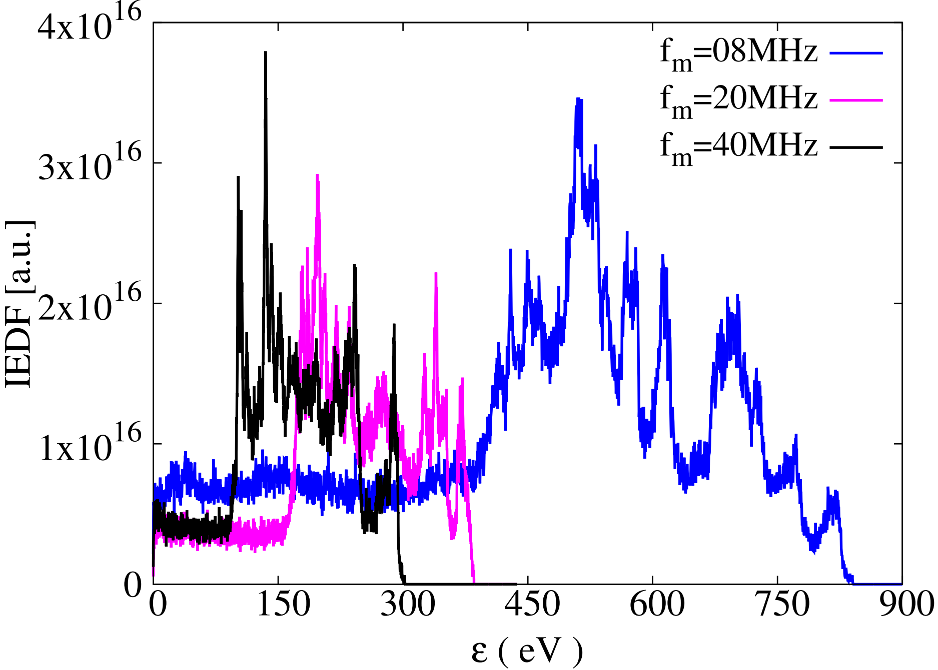

4x10^16
3x10^16
2x10^16
1x10^16
0
IEDF [a.u.]
0
150
300
450
600
750
900
ε (eV)
f_m=08MHz
f_m=20MHz
f_m=40MHz

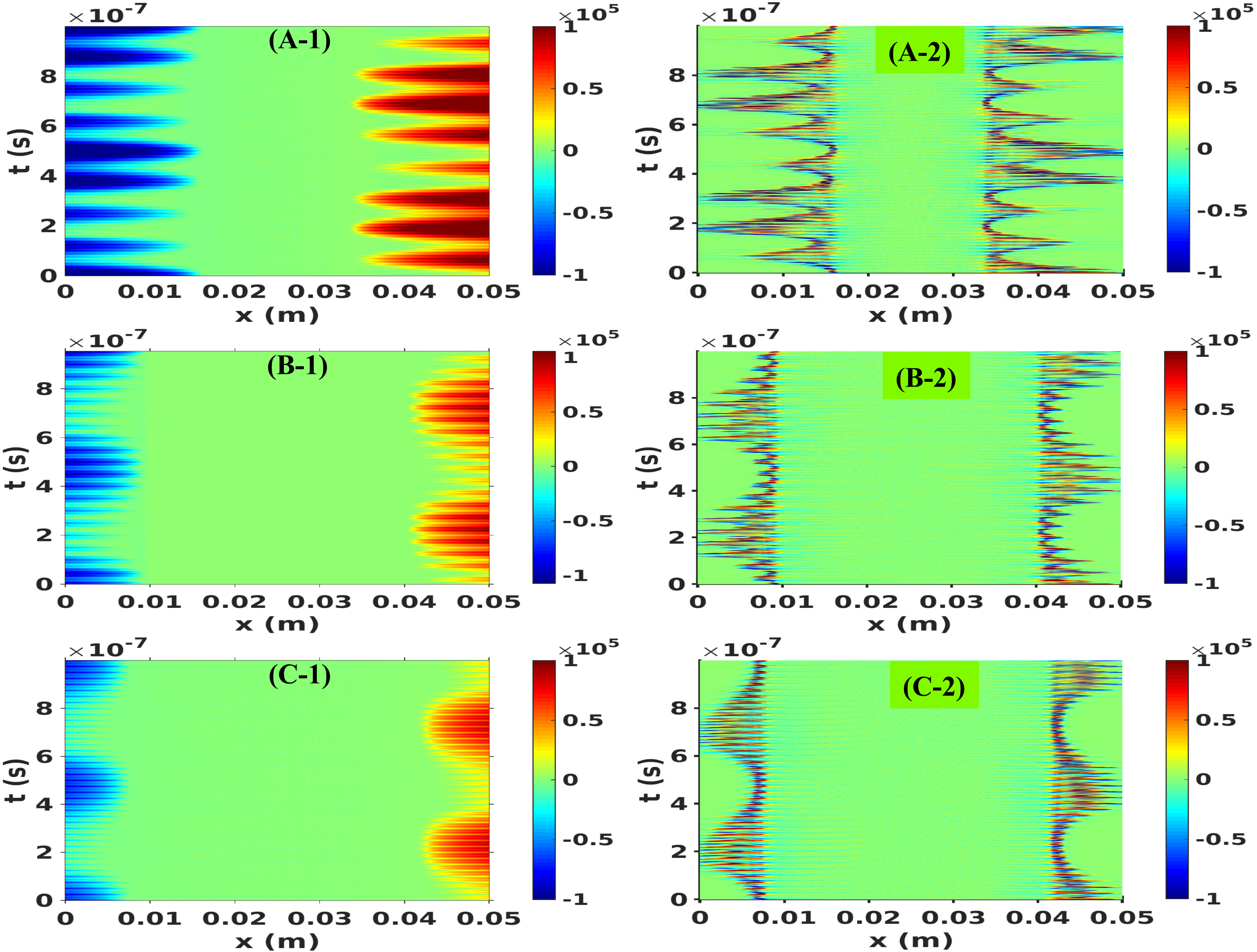
(A-1)
(A-2)
(B-1)
(B-2)
(C-1)
(C-2)
t (s)
x (m)
×10^-7
×10^5
0
2
4
6
8
0.01
0.02
0.03
0.04
0.05
1
0.5
-0.5
-1

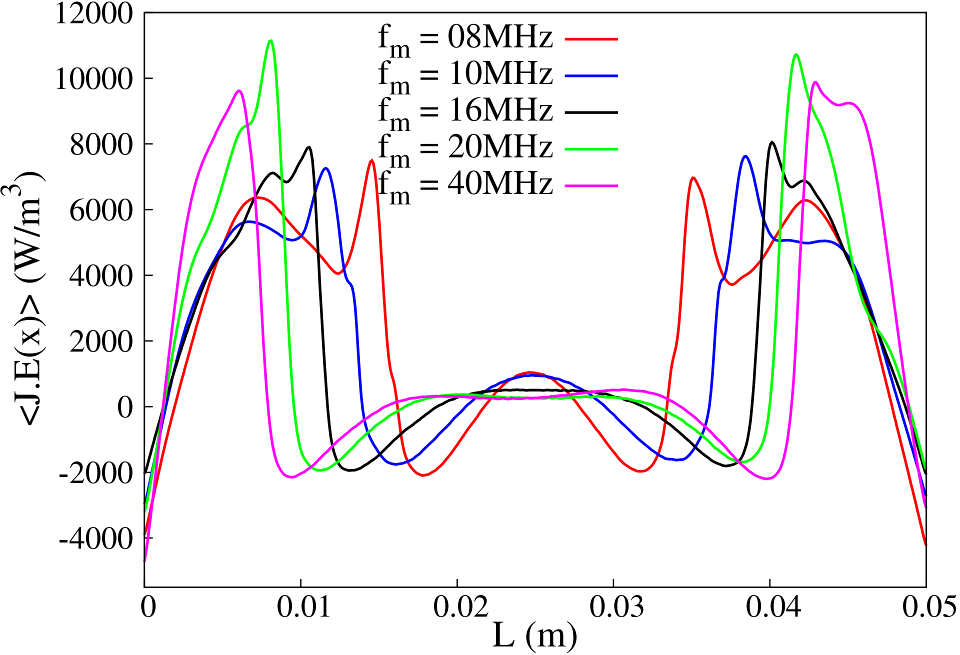

f_m = 08MHz
f_m = 10MHz
f_m = 16MHz
f_m = 20MHz
f_m = 40MHz
<J.E(x)> (W/m^3)
12000
10000
8000
6000
4000
2000
0
-2000
-4000
0
0.01
0.02
0.03
0.04
0.05
L (m)

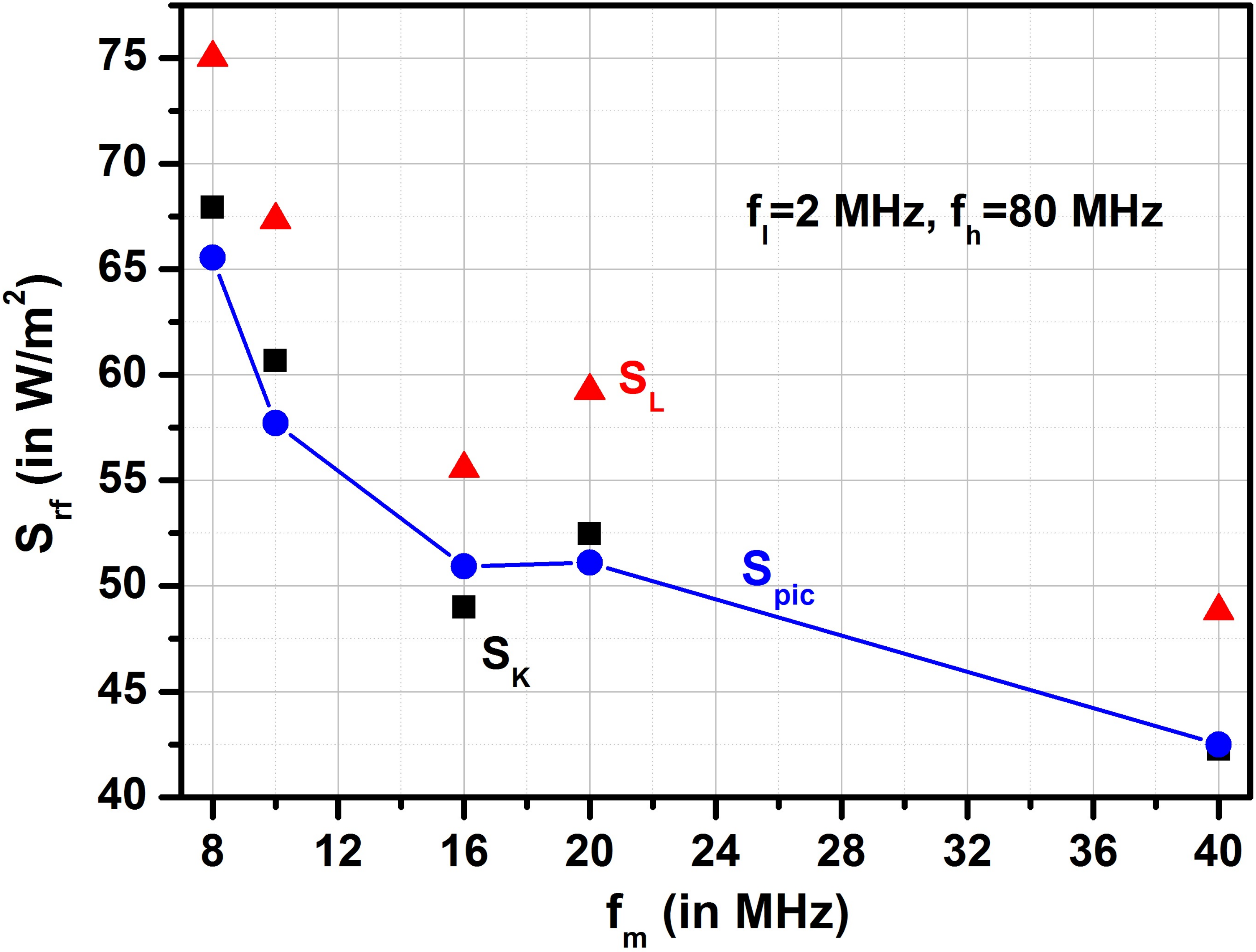
S_{rf} (in W/m^2)
f_m (in MHz)
f_l=2 MHz, f_h=80 MHz
S_L
S_K
S_{pic}
40
45
50
55
60
65
70
75
8
12
16
20
24
28
32
36
40